

Adsorption of Methylene blue and Methyl orange on nano zero-valent iron (nZVI) coated biochar: column adsorption experiments

Wenchuan Ding^a, Alphonse Habineza^{a,b,*}, Xiaolan Zeng^a, Zhuoyi Yan^a, Jun Yan^a, Guang Yang^a

^aFaculty of the Built Environment, School of Urban Construction and Environmental Engineering, Department of Environmental Engineering, Key Laboratory of Three Gorges Reservoir Region's Eco-Environment, Chongqing University, Chongqing 400045, China, Tel. (+250)788-816-695; emails: ahabineza@mkurwanda.ac.rw/habialpha@gmail.com (A. Habineza), dingwenchuan@cqu.edu.cn (W. Ding), 276686704@qq.com (X. Zeng), 540308299@qq.com (Z. Yan), 337385362@qq.com (J. Yan), yangguang_sunshine@qq.com (G. Yang)

^bSchool of Health Sciences, Department of Public Health, Mount Kenya University Rwanda, Republic of Rwanda

Received 26 November 2021; Accepted 27 March 2022

ABSTRACT

Despite its attractiveness and combinatorial effectiveness, the biochar supported nanoscale zero-valent iron particles (nZVI) composite has not been applied in a multi-dye system and fixed bed column experiments. The present work aimed at preparing a corn cob biochar coated with nZVI particles to obtain an efficient low-cost adsorbent and investigate its potential to remove two synthetic dyes Methylene blue (MB) and Methyl orange (MO) from their single and mixture using column experiments. Brunauer–Emmett–Teller surface analyzer, scanning electron microscopy-energy-dispersive X-ray analysis, X-ray diffraction, Zetasizer Nano ZS90 and Fourier-transform infrared spectroscopy have been used to investigate the physico-chemical properties of the prepared adsorbent and explore the dynamics of competition, selectivity and adsorption mechanisms involved in dyes removal from their mixture. The MB antagonistic action vis-à-vis MO removal was high in column binary dye adsorption experiments. Experimental data of MB removal were fitted to non-linear Thomas and Yoon–Nelson models, the former fitting the best with $R^2 = 0.9886$. The dynamic absorption capacity (q_b) was 15 mg/g, the column removal efficiency 89.64% and the highest adsorption capacity 118.056 mg/g. Dyes' adsorption mechanism involved mainly electrostatic attractions, adsorbent surface sorption and pore diffusion. The complexity of the breakthrough curve of MO and non-attainment of the bed column exhaustion time suggest further detailed research studies.

Keywords: Nano zero-valent iron coated corncob biochar; Synthetic organic dyes; Methylene blue; Methyl orange; Single and binary dye column adsorption

1. Introduction

High level pollution of water resources by synthetic dyes is perceived as the most challenging environmental threats affecting human beings and entire ecosystem [1,2]. Synthetic dyes represent more than 60% of all manufactured and commercialized dye structures [3,4],

Methyl orange (MO) and Methylene blue (MB) being the most widely produced and industrially used synthetic dyes. MO is an anionic azo dye due to the presence of chromophore groups ($-N=N-$) [5,6] in its chemical structure while MB is a cationic phenothiazine dye. Textile industries are the most synthetic organic dyes' consumers [1] and greatest polluting industries [5]. While the total

* Corresponding author.

annual synthetic dye production is estimated at more than 100 million tons [5], about 11%–15% of this amount is lost during the dyeing process and therefore indiscriminately released into the aquatic environment [5,7]. Once in water bodies, synthetic dyes significantly reduce the photosynthetic activity, affecting the functioning of aquatic ecosystem [8,9]. Dyes reduce the light penetration, impeding the photosynthesis of aquatic flora and also decrease the amount of dissolved oxygen, which in turn, affect the life of aquatic living organisms [7,10,11]. On the other hand, the colored water due to the presence of dyes has always been causing aesthetic problem and undesirable for industrial and domestic use even at very low dye concentrations [12]. From the toxicological view point, synthetic dyes not registered as “safe dyes” for consumption have been reported to cause food safety and health problems which forced many governments across the world to introduce strict legislations and food adulteration acts [13]. Despite controversies and discrepancies among research results, some studies have shown that synthetic dyes were responsible of hyperactivity, restlessness, and sleep disturbance in children, cancer and allergies-causing to human beings [13]. Workers in the dye manufacturing industries were found to develop bladder cancer [10]. When entered the food chains, dyes provide bio-magnification, contaminating heavily organisms at higher trophic levels [10]. Heavy metals entering in the composition of synthetic dyes can be easily assimilated by the fish gills [10] and affect the trophic chain including human beings via fish eating. Beyond their recalcitrance properties and long half-life, azo dyes and their derivative compounds have shown to cause adverse impacts to soil bacterial population. Oxidative stress properties of chromium (entering the composition of the textile dyes) negatively affect the germination and growth of plantations [10]. Like other synthetic organic dyes, MB and MO are highly toxic, carcinogenic, mutagenic and teratogenic to animals and human beings due to the presence of aromatic and $-N=N-$ groups in their molecules [1,6,11]. MB was reported to cause irritation, gastritis, diarrhea, cyanosis, tissue necrosis, jaundice and vomiting in humans [1,7,14]. In addition, many side effects such as headache, vomiting, confusion, breathing impairment and dysfunction, high blood pressure, serotonin syndrome, red blood cell breakdown, and allergic reactions were attributed to this MB contaminant. Furthermore, when taken up into human body, MB may reduce the ferric ions in haemoglobin to ferrous ions [15]. MO on the other hand causes allergy when in contact with skin leading to skin eczema and can be poisonous once swallowed [16].

High toxicity and deleterious effects of the synthetic dyes alongside with their non-biodegradability [9], high physical and chemical stability [4] and their persistence into the environment have always stimulated the imperative need to solve the big problem of water coloring and environmental pollution by dyes. A variety of techniques and methods including chemical redox reaction [1], membrane filtration [17,18], coagulation and photo-catalysis [19], ion exchange, adsorption [11] have been applied to eliminate dyes from the polluted waters. Unfortunately, the main drawbacks of many of these methods have been

high costs, much energy consumption, associated secondary pollution and much toxic sludge production [1]. Only adsorption technology has attracted many scientists and researchers due to its relative low cost among other wastewater treatment methods [20], less sludge production, simple design and operation [21], rapidity and high potential to remove a wide range of contaminants from aqueous solutions. The technology has been highly appreciated and widely used due to the quasi-absence of side effects and/or toxicity to water and higher efficiency in comparison with other conventional treatment methods [5]. Furthermore, adsorption technique was proven to be the most responsive method to the high demand of treatment of massive volumes of industrial waste waters [20]. It has revealed itself to be the best alternative cost-effective and economically viable treatment method especially when adsorbents are not expensive and readily available [5,20]. Moreover, the technology has been in use since 450 BC through the use of charcoal for drinking water purification [22].

The limited porosity and low effectiveness of the charcoal prompted the production of an activated carbon in 1822 from the raw carbonaceous materials. This paved the way for the commercial applications of activated carbon and gained a growing worldwide importance on industrial scale application throughout 19th and 20th centuries [22]. Many commercial adsorbents such as silica gels, organic gels, activated alumina and zeolites have been used to remove a wide range of contaminants from industrial effluents and shown a high efficiency [23,24]. However, extensive use and growing industrial demand of this activated carbon coupled with the high production costs [22,23] and the 2000s economic crisis prompted many scholars and researchers to turn their interest [25] in the development of biochar-based adsorbents. This carbon-rich residue is produced from various low-cost biomass materials such as wood chips, crop residue, or manure via a high temperature (300°C – 950°C) pyrolysis in a low or absence of oxygen environment under atmospheric N_2 [26,27]. Biochars derived from some waste biomass such as wheat straw [12], sugarcane bagasse [28], papaya seeds [29,30], maize stem tissue [4] and swede rape straw [15] demonstrated a relatively high adsorption capacity in removing many contaminants including organic dyes from polluted waters. Compared to the activated carbon, the biochar was found to be of low-cost and have a comparable or higher adsorption capacity than the activated carbon [31]. In addition, being a renewable adsorbent, biochar presents an economic and environmental benefits and is still considered as a promising potential resource for environmental technology used for water contaminants removal [31]. Good biochar adsorptive properties were attributed to many functional groups and mineral components, large specific surface area and porous structure on the biochar surface [20,31]. Despite these excellent properties, recent scientific efforts aimed to improve adsorptive properties of the raw biochar via appropriate modification methods have shown that the engineered biochar had stronger adsorption capacity than the pristine biochar [32]. One of the most emerging, innovative and promising modification method is the combination of the biochars (BCs) and nanotechnology, the nanoscale zero-valent metals (nZVMs) particularly the nano zero-valent iron (nZVI)

particles [33]. The combination of biochar and nanotechnology continues to gain a growing interest among researchers. It yields a biochar-based nanocomposite (nZVI/BC) with excellent adsorptive qualities mainly larger specific surface area with more active adsorption sites, enhanced porosity with good pore-size distribution and pore volume, higher cation exchange capacity (CEC), greater thermal stability and many functional reactive groups, improved oxido-reductive and catalytic degradation ability and magnetic properties [32,34,35]. The combinatorial effect has also shown to overcome some of individual technology drawbacks. For instance, the ferromagnetic properties of new composite adsorbent allow an easy separation of adsorbent from aqueous solution using a simple magnet and the adsorption capacities of the pristine biochar get strengthened [32,33,36–39]. The biochar provides an excellent support for the dispersion and stabilization of the nZVI particles, enhancing their catalytic ability, high contaminant adsorption and degradation in solutions [26,37,40].

Many review papers [32] and research articles [34,37] have reported the impregnation of nZVI particles onto BC surface and exploration of enhanced adsorptive properties of the new engineered composite in environmental remediation, especially the removal of persistent contaminants including organic dyes. Though this type of engineered material was suggested as an alternative and innovative adsorbent [32], the above-discussed properties were not fully investigated for the removal of the synthetic dyes from a multi-dye system and complex wastewater mixture. On the other hand, most of the research studies on dyes' removal from wastewaters by nZVI/BC have been conducted in a single contaminant system in batch experiments, providing fundamental skills but leaving a huge gap for practical application at the large industrial scale. Investigative studies on synthetic dyes adsorption by nZVI/BC in a multi-pollutant system and fixed bed column experiments are very limited across the literature. Therefore, new insights of the bio-sorbent behavior in a multi-contaminant adsorption

system, dynamics, mutual influence and adsorption mechanisms involved are still to be acquired. To bridge this research gap, the current study aims at preparing a corn cob biochar coated with nZVI particles to obtain an efficient and environmentally friendly low-cost adsorbent nZVI/BC composite and investigate its potential to remove two synthetic dyes Methylene blue (MB) and Methyl orange (MO) from their single and mixture in water using column experiments. The physico-chemical characterization of the modified biochar was investigated using Brunauer–Emmett–Teller (BET) surface analyzer, scanning electron microscopy-energy-dispersive X-ray analysis (SEM-EDX), X-ray diffractometers (XRD), Zetasizer Nano ZS90, Fourier-transform infrared spectrometer (FTIR) to explore the dynamics of competition, selectivity and adsorption mechanisms involved in their mixture.

2. Materials and methods

2.1. Adsorbent preparation and characterization

The dried corncobs obtained from Bishan County of Chongqing Municipality, China, were first washed with tap water to remove impurities and then dried at ambient temperature for one week. They were pyrolyzed in a muffle furnace at 600°C following the methods described in the literature [37,38] to obtain the corn cob biochar (BC). Prior to pyrolysis process, the furnace was filled with N₂ (600 mL/min) and maintained oxygen free throughout the reaction. After cooling down to room temperature, the BC residue was taken out from the device, crushed to 50–300 mesh size using grinder (BJ-100, Baijie Ltc.) and finally screened to 30 μm sieving. The obtained corncob biochar, referred to BC₆₀₀, was stored in a container at 4°C for further research.

The synthesis of nZVI coated onto biochar (nZVI/BC composite) was performed according to the method described by Shang et al. [41] and Sun et al. [42] with some modifications. Typically, the pre-determined amount of iron (FeCl₃·6H₂O) was dissolved in an appropriate

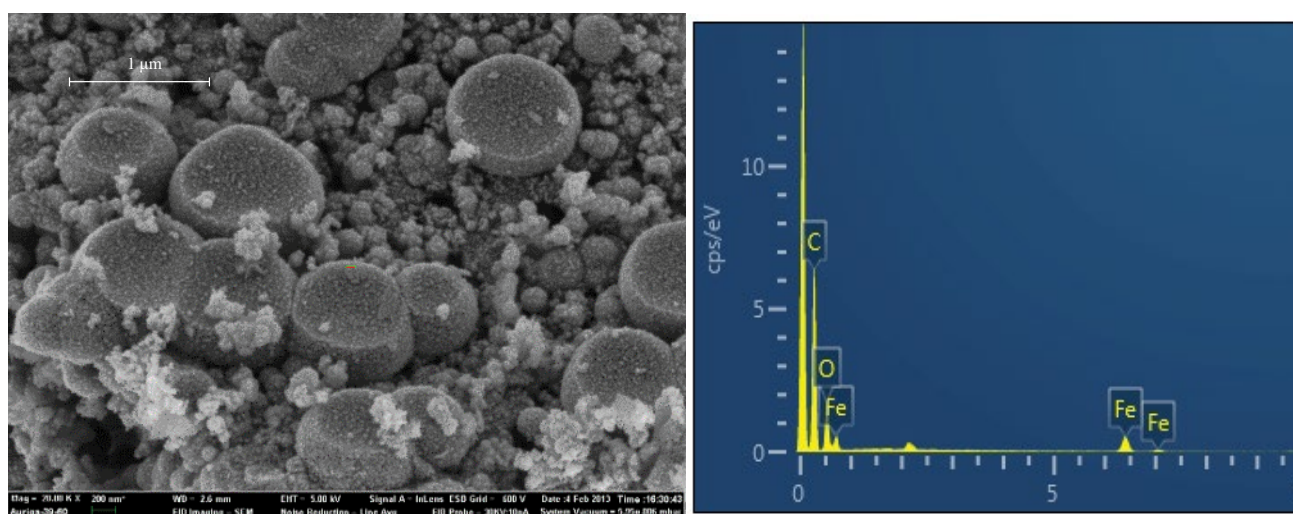
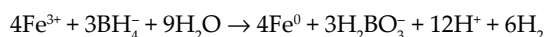


Fig. 1. SEM-EDX measurement of BC after nZVI coating.

quantity of solvent (ethanol/deionized water (3/7, v/v) and added into the designed mass of corncob biochar in a 500 mL beaker (Fe/BC impregnation mass ratio of 1:5). The beaker was immersed into a thermal-controlled heater with a magnetic stirrer (DF-101S, Bangxi Instrument Technology (Shanghai) Co., Ltd.) while maintaining the temperature at 23°C. The stirring time and stirring rates were set at 89.99 min and 400 rpm respectively. At the end of the mixing and homogenization process, sodium borohydride (NaBH₄) solution (with concentration equivalent to 4 times higher than that of Fe³⁺) was added dropwise under the same above stirring conditions at a titration rate of 0.625 mL/s. While adding the NaBH₄ solution, a plenty of gas was bubbled out and the mixture solution immediately turned black. The NaBH₄ solution reduced the ferric chloride (Fe³⁺) into zero-valent iron (Fe⁰) in aqueous phase according to the reaction. All solvents were degassed and saturated with N₂ for more than 1 h before being used and the whole synthesis process was carried out under the N₂ environment.



The composite particles (black precipitate) generated was separated from the liquid phase by vacuum filtration then washed with deionized water (>100 mL/g) followed by diluted ethanol (~5%) [43,44]. Finally, the product was oven dried at 60°C for 12 h and stored for adsorption experiments and physico-chemical characterization. BET surface analyser, scanning electron microscopy (AURIGA, Zeiss Ltd., Germany) coupled with SEM-EDX, X-ray diffractometer (D/Max-IIIIC, Nippon Science Desk Co., Ltd., Japan), Fourier Transformed Infrared Spectroscopy (Nicolet iS5, Thermo Fischer Scientific Ltd., USA), Zetasizer Nano ZS90 (Malvern, U.K) were used to determine properties of the newly synthesized adsorbent (nZVI/BC composite) before and after adsorption experiments.

2.2. Reagents and adsorbate aqueous solutions

All chemical reagents used throughout the experimental work were of analytical grade and purchased from Chongqing Chuandong Chemical (Group) Co. Ltd. and Chengdu Kelon Chemical Reagent Factory, China while the deionized water (18.25 MΩ) was prepared in the laboratory using a Standard Ultrapure Water Machine (WP-UPT-10, Fupure Co., Ltd., China). Synthetic dyes containing wastewater was prepared from the stock solutions (1,000 mg/L) prepared by dissolving appropriate mass of MB and MO in deionized water. The working aqueous dye solutions (100 mg/L) were prepared by a suitable serial dilution from the stock solutions. Adjustment of the solution pH was done by addition of HCl (0.1 M) or NaOH (0.1 M) and was measured using a pH-meter (PHS-3E-INESA).

2.3. Column adsorption experiments

A laboratory scale glass column with a height of 10 cm and an internal diameter of 1.6 cm with a 0.2 cm layer of sintered discs made of Pyrex borosilicate glass was used to perform experiments of dyes adsorption in a continuous flow fixed-bed column. An adsorbent mass of 1.0 g of

nZVI/BC (1:5) (equivalent to about 2.0 cm of bed depth) was introduced in the column between glass wool which prevented it from being washed out and enabled a uniform inlet flow into the column. The column was operated at room temperature (20°C–25°C). A micro flow multi-channel peristaltic pump (BT-100 EA) was used to pump the dye's aqueous solution into the column bottom (down flow mode) at 100 mg/L of dye influent concentration (both single and binary dye system), 10 mL/min of the flow rate, pH = 3.0 for MO single dye removal and binary dye system (MO + MB). In MB single dye system, the pH was set at 7.0. Cylindrical plastic bottles were used for dyes effluent sample collection at a regular time interval throughout the adsorption process. The flow of the column was continued until the dye outlet concentration (C_t) was close to its influent concentration (C_o), that is, C_t ≥ 99% C_o. All experiments were conducted in duplicate and the mean value of the results was calculated. UV-Visible spectrophotometer (T6, Purkinje General Instrument Co., Ltd) was used to measure the remaining dye's concentrations.

Adsorption efficiency (E) of the column experiment was determined using the formula [1]:

$$E = \left(1 - \frac{C_t}{C_o}\right) \times 100 \quad (1)$$

where C_t being the outlet dye concentration (mg/L) at time t, C_o = initial dye concentration (mg/L).

The dynamic uptake capacity, Q_{bed} (mg/g) was computed as follows [45]:

$$Q_{\text{bed}} = \frac{M_r}{m} \quad (2)$$

where m stands for the packed adsorbent (g), M_r is the difference between the inlet and outlet dye concentration (mg/L). M_r is obtained according to the equation:

$$M_r = V_e \cdot C_o - \frac{\sum (V_{n+1} - V_n)(C_{n+1} - C_n)}{2} \quad (3)$$

where V_e (L) is the volume of effluent at column exhaustion time, C_o (mmol/L) the inlet dye concentration, V_n (L) is the effluent volume at the nth reading; V_{n+1} (L) is the effluent volume at the (n+1)th reading, C_n (mmol/L) the outlet dye concentration at nth reading and C_{n+1} is the outlet concentration at the (n+1)th reading (mmol/L). At the time when the dye outlet concentration is equal to 1% of that of its inlet concentration entering (at 1% breakthrough), the adsorbed amount (Q_b) is given by the following relation [45]:

$$Q_b = \frac{Q \cdot t_1 \% \cdot C_o}{1,000 \cdot m} \quad (4)$$

where Q = flow rate, t₁% is column service time (min), C_o = inlet dye concentration and m is the adsorbent packed amount (g).

2.3.1. Column adsorption models and equations

The description of the column performance and breakthrough curve was based on two known models namely Thomas and Yoon–Nelson models [45–47] using their non-linear equations. The non-linear regression equation was found to be the best fitting the model parameters and reliable tool for adsorption modelling, leading to less experimental errors at different error magnitudes and minimized statistical errors [47–49].

$$\frac{C_t}{C_o} = \frac{1}{1 + \exp\left[\frac{K_{Th}}{Q} \cdot (Q_{max,m} - C_o V_t)\right]} \quad (5)$$

(Non-linear form of Thomas model)

$$\frac{C_t}{C_o} = \frac{1}{1 + \exp(k_{YN} \tau - k_{YN} t)} \quad (6)$$

(Non-linear form of Yoon–Nelson model)

where K_{Th} is the Thomas rate constant (mL/mg min), Q_{max} is the maximum concentration of the adsorbate (mg/g), V_t (mL) is the effluent volume, m the adsorbent mass (g), C_t is the outlet dye concentration (mg/L) at time t , C_o is the inlet dye concentration (mg/L) and Q is the linear velocity (mL/min). The Thomas model assumes that the adsorption process obeys the Langmuir kinetics of adsorption–desorption and the rate driving force conforms to the second-order reversible reaction kinetics. Furthermore, the model considers that the adsorption process is not controlled by the chemical reaction but regulated by the mass transfer at the interface. In the Yoon–Nelson model, τ is the theoretical time (min) required to accomplish 50% adsorbate breakthrough and k_{YN} is the Yoon–Nelson rate constant (min^{-1}). The Yoon–Nelson model assumes that the contaminant adsorption probability rate decreases proportionally with its sorption and the breakthrough on the adsorbent material.

The column data were fitted to the two non-linear models by plotting C_t/C_o against time t (Thomas model) or $C_t/(C_o - C_t)$ vs. sampling time (t) (Yoon–Nelson model). The model parameters ($K_{Th}C_o$ and k_{YN}) and ($K_{Th}Q_{max}m/Q$ and τ) were computed from the slope and intercept respectively [46,48,50,51]. To construct the dye breakthrough curve, the ratio C_t/C_o was plotted vs. the time or volume of the effluent collected in the course of time [47,51,52].

3. Results and discussion

3.1. Physico-chemical characterization of adsorbents (biochar and nZVI/BC)

The measured surface area of biochar was 64.590 m^2/g while it was reduced to 49.309 m^2/g as a result of nZVI coating onto biochar. In contrast, the biochar total pore volume increased from 0.0553 to 0.0972 cm^3/g . This increase was probably due to the accommodation of iron particles within biochar pores and hence, augmenting the biochar porosity [19,43]. The results of SEM-EDX indicate

many cracks, irregular and rough structures of the pristine biochar surface which became relatively smooth and polished after biochar modification, indicating that the dispersion of the iron particles was effective (Fig. 1). From Fig. 1, it can be seen that the nanosphere nZVI particles adhered one another linearly oriented due to the magnetic properties of the Fe particles whose diameters were previously found to be ranging from 50 to 100 nm [19]. The EDX images indicate that after BC modification, the proportions of iron particles rose from 0.17% to 16.79%, oxygen from 12.55% to 21.125% while the carbon decreased from 86% to 61.50%.

The composite powder characterization by XRD (Fig. 2) has revealed the successful synthesis of the nZVI at nanoscale level (<100 nm). For instance, the peaks located at $2\theta = 44^\circ\text{--}45^\circ$ are characteristic of the nanoscale zero-valent iron particles ($\alpha\text{-Fe}$) as reported in many literature [4,53]. Strong peaks at $2\theta = 35.74^\circ\text{--}35.9^\circ$ are more likely to be the iron oxides mainly Fe_3O_4 and $\gamma\text{-Fe}_2\text{O}_3$ [54]. The adsorbent surface charge (zeta potential [ζ potential]) measured over a solution pH range of 2.1–9.2 at 25°C shows that the values of the zeta potential of the nZVI/BC₆₀₀ decreased from +48.3 to –30.1 mV (Fig. 3). In the studied pH range, the zeta potential values are positive until the pH value of about 5.8 and negative for the rest of the pH range. The BC₆₀₀ zeta potentials values are all negative in the pH range and vary from –59.5 to –73.1 mV. The biochar zeta potential change from negative to positive after biochar modification might have resulted from the interactions between BC and nZVI particles.

3.2. Column adsorption experiments

3.2.1. Column adsorption in single dye system

The column adsorption break point appeared after 15 min of the column service time, outlet effluent concentrations being 6.20 and 10.36 mg/L for MO and MB, respectively. The MB removal gradually declined, suggesting a progressive exhaustion and saturation of the bed column binding sites (Fig. 4). The column bed exhaustion

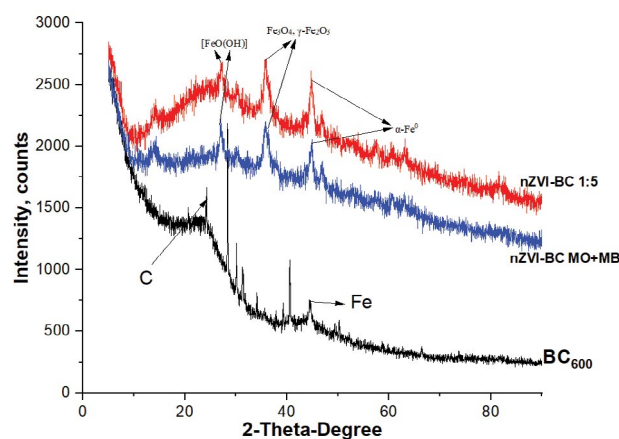


Fig. 2. XRD patterns of the pristine BC₆₀₀, modified BC (nZVI/BC) and nZVI/BC-MO + MB.

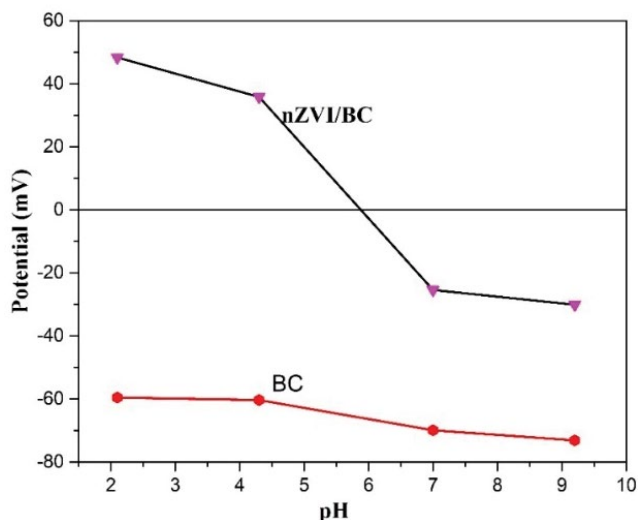


Fig. 3. Zeta potential of the BC and nZVI/BC at different pH values at 25°C.

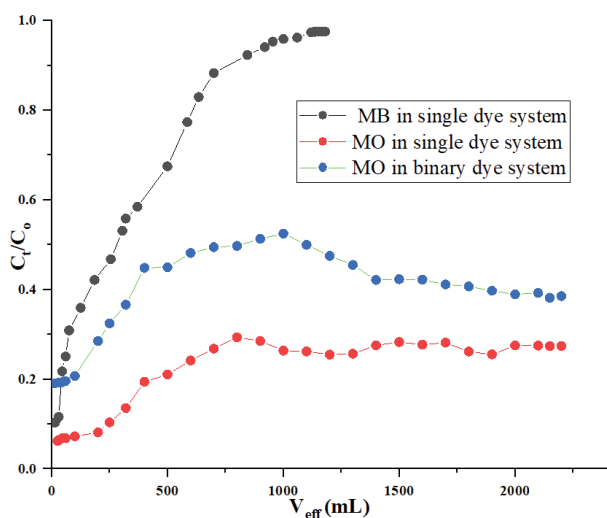


Fig. 4. Breakthrough curves of MO and MB column adsorption by nZVI/BC (1:5) in a single and binary dye system (adsorbent dose = 1.0 g, pH = 3.0; MO and pH = 7.0 for MB; conc. 100 mg/L each dye; flow rate = 10 mL/min, room temperature).

time was reached after 10 h of the column service time, the outlet effluent concentration was 98% of its influent concentration. Similar trend results were obtained for MB and MO by carboxylated diaminoethane sporopollenin (CDAE-S) [55] in a bed-fixed column studies. In contrast, MO concentration was gradually becoming more coloured, suggesting an increase of the outlet effluent concentration with time as revealed by UV-Vis spectrophotometer measurements. After 10 h of the column service time, the highest outlet effluent concentration was 29.38 mg/L. From this time there has been a slight continuous decrease and increase of outlet effluent concentration up to 22 h when the dye volume of 2,200 mL was exhausted (Fig. 4). The monitoring of the pH in the MO column studies shows

that the pH raised from 3.0 to 5.70 to finally decline up to the pH value of 3.20. The observed trends of MO could be a result of pH fluctuation and the reversibility of the reaction as previously proven in the literature [33]. It was observed that during the cleavage of the azo N=N bond by the Fe^0 particles, the hydrazine-like N-H single bonds are formed which, subsequently, consume the H^+ and therefore the pH raises. Furthermore, Fe^0 could react with water to generate Fe^{2+} , H_2 and OH^- . The latter hydroxide ions were reported to be responsible of the raise of the solution pH. The generated ferrous ions are susceptible to combine with OH^- , leading to the decrease of the solution pH [33].

3.2.2. Column adsorption in binary dye system

The coexistence of MB with MO in aqueous solution mixture significantly impacted the MO removal. The UV Vis spectrophotometer measurement has revealed that the first collected outlet effluent concentration of MO was approximately 20 mg/L against 6.20 mg/L in single dye system, suggesting an inhibitory effect of MB towards the MO removal and a higher affinity of the corn cob bio-char-based adsorbent to MB than MO. It seems that the dye MB is first adsorbed onto the nZVI/BC due to the affinity of the adsorbent to cationic dyes (MB) than anionic dyes (MO) as previously reported [4]. Another plausible reason could be the solution pH raise accompanying the removal of MO [33] which in turn, affected the zeta potential of the adsorbent surface as observed in the present work. The increase in pH changes the zeta potential of the adsorbent surface, becoming more negative (Fig. 3) and hence exerting an electrostatic attraction with the cationic dye (MB) and repulsion with anionic dyes MO. Gong et al. [56] observed a more favorable adsorption of MB onto the surface of GO-sand than that of Pb(II) as a result of π - π interactions between MB and GO on sand surface in packed filter. Furthermore, the higher outlet effluent concentrations of MO in binary dye system than in single dye system (Fig. 4) again reinforces the affinity and preference of the nZVI/BC to the MB than MO. Nevertheless, in both cases the adsorbent exhaustion point could not be reached until 22 h of the column operation time as it can be seen from the MO breakthrough curves in Fig. 4. In contrast, the trends of the breakthrough curves and behavior of MB observed in column single dye adsorption were the same as in column binary dye system adsorption.

3.2.3. Evaluation of the column performance

The performance of the packed bed column is normally evaluated between the breakthrough and adsorbent exhaustion points [57]. In the present work, given that the MO exhibited an abnormal breakthrough curve due to the reversible reaction, instability of the formed intermediates or impurity of the substance (MO), it was not possible to evaluate the performance of the packed bed column. In contrast, the column data and breakthrough curve analysis for MB adsorption were modeled by the nonlinear forms of Yoon-Nelson and Thomas pragmatic models and results are presented in Fig. 5. The computed values of the two models' parameters are tabulated in Table 1 and indicate the best

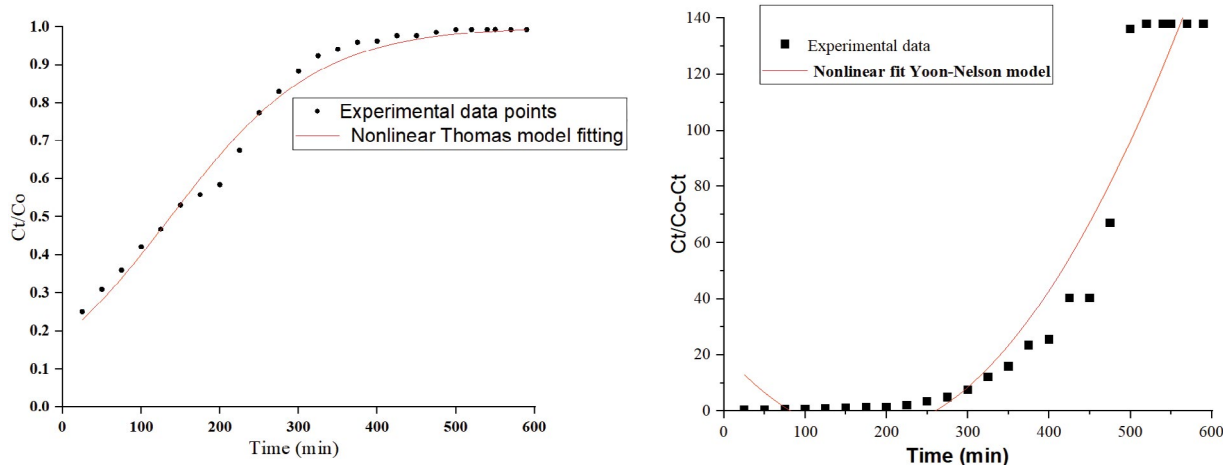


Fig. 5. MB breakthrough curve modeling by Thomas model (a) and Yoon–Nelson model (b).

Table 1

Parameters of Thomas and Yoon–Nelson models for the sorption of MB by nZVI/BC (1:5)

| Adsorbent | Bed height (cm) | Flow rate (mL/min) | Thomas model | | Yoon–Nelson model | | | q_b (mg/g) | Q_{\max} (mg/g) |
|---------------|-----------------|--------------------|----------------------|--------|-------------------|-----------|--------|--------------|-------------------|
| | | | K_{Th} (mL/mg min) | R^2 | k_{YN} (L/min) | i (min) | R^2 | | |
| nZVI/BC (1:5) | 2 | 10 | 0.0202 | 0.9886 | 1.5303 | 4.0312 | 0.9732 | 15.0 | 118.056 |

fit with Thomas than Yoon–Nelson model, suggesting that the rate driving force obeys the second-order reversible reaction kinetics and adsorption process is regulated by mass transfer at the interface. Both values of R^2 being greater than 0.97, it is an indication that the two models (Thomas and Yoon–Nelson models) fit well the experimental data and therefore, can effectively predict the MB adsorption performance in a fixed bed column [56]. Our findings are consistent with the results by Gong et al. [56] who observed a better fitting of Thomas model than Adams–Bohar model for MB adsorption in a bed-fixed column. However, when comparing the linear fitting of Thomas and Yoon–Nelson models, these authors found that the experimental data for Methylene blue adsorption in fixed-bed column were best fitted with the Yoon–Nelson model than Thomas model [56].

According to the experimental data (outlet effluent concentrations) recorded at different time intervals and based on the information provided by the breakthrough curve, the breakthrough time and exhaustion time were found to be 15 and 590 min respectively (Fig. 6). In addition, the present study has found the q_b to be 15 mg/g at 10% breakthrough point (results are presented in Table 1). Moreover, the MB removal efficiency of the column was found to be 89.64% while the maximum adsorption capacity was determined as 118.056 mg/g. This column adsorption capacity is higher and/or comparable to the adsorption capacities reported in some previous research studies for MB and other dyes' removal as illustrated by the Table 2.

3.3. Dyes adsorption mechanisms

The analysis of FTIR spectra before and after dye adsorption has revealed the absorption bands in the region

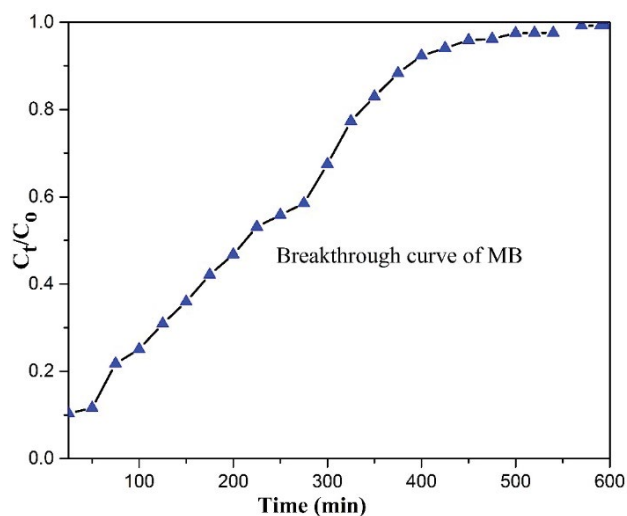
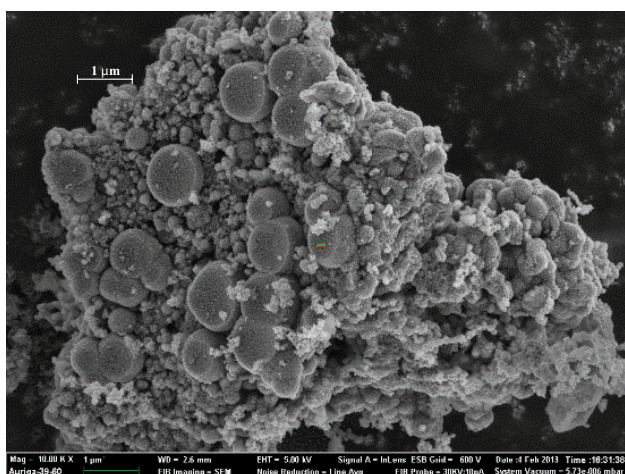


Fig. 6. Experimental breakthrough curve of MB column adsorption (pH = 7.0; init. conc. = 100 mg/L; flow rate = 10 mL/min; nZVI/BC dosage = 1.0 g).

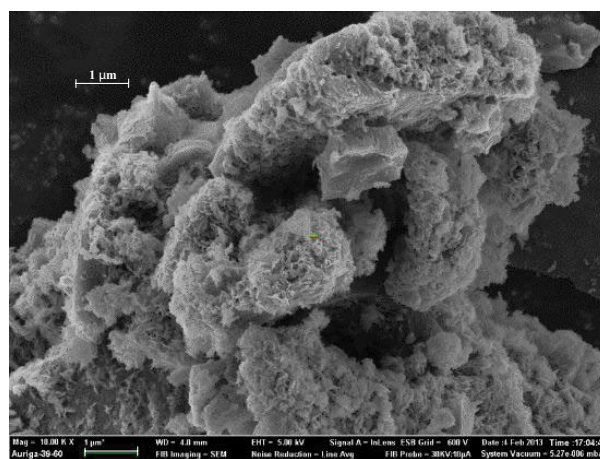
2,300–1,990 cm^{-1} assigned to several functional groups mainly the multiple bonded nitrogen compounds principally cyanides (nitriles), cyanates, isocyanates, thiocyanates, diazo and alkyne groups [62]. These chemical groups are endowed with lone pair of electrons (Lewis bases), suggesting the adsorption process to occur predominantly on the adsorbent surface [63]. Large zone of 1,100–900 cm^{-1} belonging to the silicate ions and phosphate ions and bands located in the range of 1,420–1,300 cm^{-1} could be assigned

Table 2
Comparison of column adsorption capacities (Q_{\max}) of various adsorbents

| Adsorbent | Studied contaminant | Q_{\max} (mg/g) | References |
|--|---------------------|-------------------|------------|
| Free <i>Nelumbo nucifera</i> leaf | Congo red dye | 1.179 | [58] |
| Immobilized <i>Nelumbo nucifera</i> leaf | Congo red dye | 0.783 | [58] |
| Red marine algae <i>Jania rubens</i> | Pb ²⁺ | 1,089.6 | [59] |
| Pine cone activated carbon | Acid blue 113 | 485 | [60] |
| Pine cone activated carbon | Acid black 1 | 286 | [60] |
| <i>Mucor rouxii</i> | Pb ²⁺ | 4.06 | [52] |
| <i>Mucor rouxii</i> | Cd ²⁺ | 1.25 | [52] |
| <i>Mucor rouxii</i> | Ni ²⁺ | 0.36 | [52] |
| Waste watermelon rind | Methylene blue | 113.5 | [61] |
| Tamarind seed powder | Acid yellow 17 | 978.5 | [61] |
| NaOH-modified rice husk | Malachite green | 101.31 | [61] |
| Graphite oxide coated sand | Methylene blue | 22.749 | [56] |
| Pumice-nZVI | Methylene blue | 4.27 | [1] |
| nZVI-coated biochar | Methylene blue | 118.056 | This work |



(a)



(b)

Fig. 7. SEM images of the nZVI/BC before dye's adsorption (a) and after dyes adsorption (b).

to carboxylate ions [62]. The multiple bonded nitrogen groups and carboxylate are nucleophiles and therefore can easily donate electrons to the cationic pollutant such as Methylene blue or H⁺ (acidic environment) [64], resulting into electrostatic attractions between dyes and adsorbent. On the other hand, results of the zeta potential measurement suggest that MO might have been also removed via electrostatic attraction mechanism due to the positive charge of the nZVI/BC₆₀₀ below pH value of about 5.8. Looking at SEM images before and after adsorption (Fig. 7) process, the two dyes might have been removed via adsorption onto adsorbent surface or sorption into adsorbent's pores (pore filling) via intra-particle diffusion mode. The observed XRD peaks corresponding to various iron oxides (Fig. 2) suggest that the two dyes may have been removed via adsorption, sorption, complexation processes as well as oxido-reduction reaction as previously indicated in the literature [12,65].

4. Conclusion

The engineered adsorbent material, nZVI/BC from the low-cost biomass corn cob was investigated for its potential for the adsorption of Methylene blue and Methyl orange in single and binary dye system through column adsorption experiments. An inhibitory effect of MB towards the MO removal was observed in binary dye system due to higher affinity of the corn cob based-adsorbent to cationic dyes (MB) than anionic dyes (MO). The column data and breakthrough curve analysis for MB adsorption were predicted by both non-linear Thomas and Yoon–Nelson models, Thomas model fitting better than Yoon–Nelson model. The dynamic uptake capacity (q_b) was found to be 15 mg/g, the column removal efficiency of MB was 89.64% while the maximum adsorption capacity was determined as 118.056 mg/g. Dyes removal might have involved the electrostatic attractions, adsorption and

sorption via intra-particle diffusion which is the adsorption limiting step. The synthesized material may be suggested as a suitable alternative potential adsorbent to effectively remove the Methylene blue from wastewaters. Corn cobs are widely accessible and low-cost biomass materials and can be used as a substitute of the expensive commercial adsorbents. Further research studies may apply the nZVI-coated onto corn cob BC to the real industrial effluents in order to make the bio-sorption process ecologically viable and understand the dynamics of dyes interactions with a complex mixture of industrial effluents. It can also be suggested further detailed column adsorption studies aiming at investigating the key column design parameters namely flow rate, bed height, adsorbent particle size, inlet concentrations to elucidate the MO adsorption-involved mechanisms.

Acknowledgment

The research is financed by the Chinese National Water Pollution Control and Treatment Science and Technology Major Project (No. 2012ZX07102-001).

References

- [1] M. Genisoglu, A.Y. Goren, E. Balci, Y.K. Recepoglu, H.E. Ökten, Pomza ve nSDD-Pomza ile Sabit Yataklı Kolon Reaktörde Metilen Mavisi Giderimi: Deneysel ve Modelleme Çalışması, Süleyman Demirel Üniversitesi Fen Bilimleri Enstitüsü Dergisi, 2019, pp. 298–305. Available at: <https://doi.org/10.19113/sdufenbed.538084>
- [2] J. Liu, F. Chen, Q. Yao, Y. Sun, W. Huang, R. Wang, B. Yang, W. Li, J. Tian, Application and prospect of graphene and its composites in wastewater treatment, Pol. J. Environ. Stud., 29 (2020) 3965–3974.
- [3] M.Y. Kilic, A comparative treatability study for textile wastewater: Agricultural waste adsorbent versus activated carbon, Pol. J. Environ. Stud., 29 (2020) 4131–4137.
- [4] V.M. Vučurović, R.N. Razmovski, U.D. Miljić, V.S. Puškaš, Removal of cationic and anionic azo dyes from aqueous solutions by adsorption on maize stem tissue, J. Taiwan Inst. Chem. Eng., 45 (2014) 1700–1708.
- [5] A. Mittal, J. Mittal, Chapter 11 – Hen Feather: A Remarkable Adsorbent for Dye Removal, In: Green Chemistry for Dyes Removal from Wastewater: Research Trends and Applications, 2015, pp. 409–457. Available at: doi: 10.1002/9781118721001.ch11.
- [6] L. Wu, X. Liu, G. Lv, R. Zhu, L. Tian, M. Liu, Y. Li, W. Rao, T. Liu, L. Liao, Study on the adsorption properties of Methyl orange by natural one-dimensional nano-mineral materials with different structures, Sci. Rep., 11 (2021) 1–11.
- [7] J. Mittal, Recent progress in the synthesis of layered double hydroxides and their application for the adsorptive removal of dyes: a review, J. Environ. Manage., 295 (2021) 113017, doi: 10.1016/j.jenvman.2021.113017.
- [8] A. Pirkarami, M.E. Olya, Removal of dye from industrial wastewater with an emphasis on improving economic efficiency and degradation mechanism, J. Saudi Chem. Soc., 21 (2017) S179–S186.
- [9] V.T. Lam, T.-U.T. Dao, H.-T.T. Nguyen, D. Thi Cam Nguyen, H.T.N. Le, H.T.T. Nguyen, S.T. Do, H.H. Loc, T. Duy Nguyen, Process optimization studies of Congo red dye adsorption onto magnesium aluminium layered double hydroxide using response surface methodology, Pol. J. Environ. Stud., 30 (2020) 679–687.
- [10] B. Lellis, C.Z. Fávoro-Polonio, J.A. Pamphile, J.C. Polonio, Effects of textile dyes on health and the environment and bioremediation potential of living organisms, Biotechnol. Res. Innovation., 3 (2019) 275–290.
- [11] D.D. Sewu, P. Boakye, S.H. Woo, Highly efficient adsorption of cationic dye by biochar produced with Korean cabbage waste, Bioresour. Technol., 224 (2017) 206–213.
- [12] D. Suteu, T. Malutan, D. Bilba, Removal of reactive dye Brilliant Red HE-3B from aqueous solutions by industrial lignin: equilibrium and kinetics modeling, Desalination, 255 (2010) 84–90.
- [13] J. Mittal, Permissible synthetic food dyes in India, Resonance, 25 (2020) 567–577.
- [14] N. Sahu, S. Rawat, J. Singh, R.R. Karri, S. Lee, J.-S. Choi, J. Reddy Koduru, Process optimization and modeling of Methylene blue adsorption using zero-valent iron nanoparticles synthesized from sweet lime pulp, Appl. Sci., 9 (2019) doi: 10.3390/app9235112.
- [15] Y. Feng, H. Zhou, G. Liu, J. Qiao, J. Wang, H. Lu, L. Yang, Y. Wu, Methylene blue adsorption onto swede rape straw (*Brassica napus* L.) modified by tartaric acid: equilibrium, kinetic and adsorption mechanisms, Bioresour. Technol., 125 (2012) 138–144.
- [16] Z.X. Chen, X.Y. Jin, Z. Chen, M. Megharaj, R. Naidu, Removal of Methyl orange from aqueous solution using bentonite-supported nanoscale zero-valent iron, J. Colloid Interface Sci., 363 (2011) 601–607.
- [17] M. Sulyman, J. Namiesnik, A. Gierak, Low-cost adsorbents derived from agricultural by-products/wastes for enhancing contaminant uptakes from wastewater: a review, Pol. J. Environ. Stud., 26 (2017) 479–510.
- [18] Y. Feng, D.D. Dionysiou, Y. Wu, H. Zhou, L. Xue, S. He, L. Yang, Adsorption of dyestuff from aqueous solutions through oxalic acid-modified swede rape straw: adsorption process and disposal methodology of depleted bioadsorbents, Bioresour. Technol., 138 (2013) 191–197.
- [19] M. Inyang, B. Gao, A. Zimmerman, M. Zhang, H. Chen, Synthesis, characterization, and dye sorption ability of carbon nanotube-biochar nanocomposites, Chem. Eng. J., 236 (2014) 39–46.
- [20] R. Yousef, H. Qiblawey, Adsorption as a process for produced water treatment: a review, Processes, 8 (2020) 1657, doi: 10.3390/pr8121657.
- [21] J.Z. Guo, B. Li, L. Liu, K. Lv, Removal of Methylene blue from aqueous solutions by chemically modified bamboo, Chemosphere, 111 (2014) 225–231.
- [22] Prof. Ferhan Çeçen, Dr. Özgür Aktaş, Chapter 1 – Water and Wastewater Treatment: Historical Perspective of Activated Carbon Adsorption and its Integration with Biological Processes, In: Activated Carbon for Water and Wastewater Treatment: Integration of Adsorption and Biological Treatment, Wiley-VCH Verlag GmbH & Co. KGaA, 2011, pp. 1–12.
- [23] A. Bhatnagar, M. Sillanpää, Utilization of agro-industrial and municipal waste materials as potential adsorbents for water treatment – a review, 157 (2010) 277–296.
- [24] P.S. Shah, Nanoporous Carbon From Corn Cobs and Its Applications, Ph.D., 2007 MU Dissertations, Chemical Engineering Electronic Theses and Dissertations (MU), 2007, pp. 74–94.
- [25] G.Z. Kyzas, M. Kostoglou, Green adsorbents for wastewaters: a critical review, Materials, 7 (2014) 333–364.
- [26] B. Li, L. Yang, C. Quan Wang, Q. Pei Zhang, Q. Cheng Liu, Y. Ding Li, R. Xiao, Adsorption of Cd(II) from aqueous solutions by rape straw biochar derived from different modification processes, Chemosphere, 175 (2017) 332–340.
- [27] L. Sun, D. Chen, S. Wan, Z. Yu, Performance, kinetics, and equilibrium of Methylene blue adsorption on biochar derived from eucalyptus saw dust modified with citric, tartaric, and acetic acids, Bioresour. Technol., 198 (2015) 300–308.
- [28] L.G. da Silva, R. Ruggiero, P. de M. Gontijo, R.B. Pinto, B. Royer, E.C. Lima, T.H.M. Fernandes, T. Calvete, Adsorption of Brilliant Red 2BE dye from water solutions by a chemically modified sugarcane bagasse lignin, Chem. Eng. J., 168 (2011) 620–628.
- [29] E.I. Unuabonah, G.U. Adie, L.O. Onah, O.G. Adeyemi, Multistage optimization of the adsorption of Methylene blue dye onto defatted Carica papaya seeds, Chem. Eng. J., 155 (2009) 567–579.

- [30] B.H. Hameed, Evaluation of papaya seeds as a novel non-conventional low-cost adsorbent for removal of Methylene blue, *J. Hazard. Mater.*, 162 (2009) 939–944.
- [31] X. Tan, Y. Liu, G. Zeng, X. Wang, X. Hu, Y. Gu, Z. Yang, Application of biochar for the removal of pollutants from aqueous solutions, *Chemosphere*, 125 (2015) 70–85.
- [32] W. Xiang, X. Zhang, J. Chen, W. Zou, F. He, X. Hu, D.C.W. Tsang, Y. Sik, B. Gao, Chemosphere biochar technology in wastewater treatment: a critical review, *Chemosphere*, 252 (2020) 126539, doi: 10.1016/j.chemosphere.2020.126539.
- [33] L. Han, S. Xue, S. Zhao, J. Yan, L. Qian, M. Chen, Biochar supported nanoscale iron particles for the efficient removal of Methyl orange dye in aqueous solutions, *PLoS One*, 10 (2015) 1–15.
- [34] X. Peng, X. Liu, Y. Zhou, B. Peng, L. Tang, L. Luo, B. Yao, Y. Deng, J. Tang, G. Zeng, New insights into the activity of a biochar supported nanoscale zero-valent iron composite and nanoscale zero valent iron under anaerobic or aerobic conditions, *RSC Adv.*, 7 (2017) 8755–8761.
- [35] X. Fei Tan, Y. Guo Liu, Y. Ling Gu, Y. Xu, G. Ming Zeng, X. Jiang Hu, S. Bo Liu, X. Wang, S. Mian Liu, J. Li, Biochar-based nanocomposites for the decontamination of wastewater: a review, *Bioresour. Technol.*, 212 (2016) 318–333.
- [36] G. Tan, W. Sun, Y. Xu, H. Wang, N. Xu, Sorption of mercury (II) and atrazine by biochar, modified biochars and biochar based activated carbon in aqueous solution, *Bioresour. Technol.*, 211 (2016) 727–735.
- [37] L. Qian, W. Zhang, J. Yan, L. Han, Y. Chen, D. Ouyang, M. Chen, Nanoscale zero-valent iron supported by biochars produced at different temperatures: synthesis mechanism and effect on Cr(VI) removal, *Environ. Pollut.*, 223 (2017) 153–160.
- [38] J. Shang, M. Zong, Y. Yu, X. Kong, Q. Du, Q. Liao, Removal of chromium(VI) from water using nanoscale zerovalent iron particles supported on herb-residue biochar, *J. Environ. Manage.*, 197 (2017) 331–337.
- [39] H. Li, Y.Q. Chen, S. Chen, X.L. Wang, S. Guo, Y.F. Qiu, Y. Di Liu, X.L. Duan, Y.J. Yu, Wheat straw biochar-supported nanoscale zerovalent iron for removal of trichloroethylene from groundwater, *PLoS One*, 12 (2017) 1–13.
- [40] L. Li, J. Hu, X. Shi, M. Fan, J. Luo, X. Wei, Nanoscale zero-valent metals: a review of synthesis, characterization, and applications to environmental remediation, *Environ. Sci. Pollut. Res.*, 23 (2016) 17880–17900.
- [41] J. Shang, J. Pi, M. Zong, Y. Wang, W. Li, Q. Liao, Chromium removal using magnetic biochar derived from herb-residue, *J. Taiwan Inst. Chem. Eng.*, 68 (2016) 289–294.
- [42] Y.P. Sun, X. Qin Li, J. Cao, W. Xian Zhang, H.P. Wang, Characterization of zero-valent iron nanoparticles, *Adv. Colloid Interface Sci.*, 120 (2006) 47–56.
- [43] Y. Yao, B. Gao, J. Fang, M. Zhang, H. Chen, Y. Zhou, A.E. Creamer, Y. Sun, L. Yang, Characterization and environmental applications of clay-biochar composites, *Chem. Eng. J.*, 242 (2014) 136–143.
- [44] H. Su, Z. Fang, P.E. Tsang, L. Zheng, W. Cheng, J. Fang, D. Zhao, Remediation of hexavalent chromium contaminated soil by biochar-supported zero-valent iron nanoparticles, *J. Hazard. Mater.*, 318 (2016) 533–540.
- [45] F.E. Soetaredjo, L.K. Ong, D.R. Widagdyo, S. Ismajji, Investigation of the continuous flow sorption of heavy metals in a biomass-packed column: revisiting the Thomas design model for correlation of binary component systems, *RSC Adv.*, 4 (2014) 52856–52870.
- [46] E. Malkoc, Y. Nuhoglu, Removal of Ni(II) ions from aqueous solutions using waste of tea factory: adsorption on a fixed-bed column, *J. Hazard. Mater.*, 135 (2006) 328–336.
- [47] M.E. González-López, C.M. Laureano-Anzaldo, A.A. Pérez-Fonseca, M. Arellano, J.R. Robledo-Ortiz, A critical overview of adsorption models linearization: methodological and statistical inconsistencies, *Sep. Purif. Rev.*, (2021) 1–15, doi: 10.1080/15422119.2021.1951757.
- [48] P. Husk, F. Column, X. Zhang, Y. Shang, L. Wang, Y. Song, R. Han, Comparison of linear and nonlinear regressive analysis in estimating the Thomas Model parameters for anionic dye adsorption onto CPB modified peanut husk in fixed-bed column, *Adv. Mater. Res.*, 781–784 (2013) 2179–2183.
- [49] M. Arellano, A discussion on linear and non-linear forms of Thomas equation for fixed-bed adsorption column modeling, *Rev. Mex. Ing. Quim.*, 20 (2021) 875–884.
- [50] L. Han, L. Qian, R. Liu, M. Chen, J. Yan, Q. Hu, Lead adsorption by biochar under the elevated competition of cadmium and aluminum, *Sci. Rep.*, 7 (2017) 1–11.
- [51] R. Hana, W. Yu, Z. Xin, W. Yuanfeng, X. Fuling, C. Junmei, M. Tang, Adsorption of Methylene blue by phoenix tree leaf powder in a fixed-bed column: experiments and prediction of breakthrough curves, *Desalination*, 245 (2009) 284–297.
- [52] G. Yan, T. Viraraghavan, M. Chen, A new model for heavy metal removal in a biosorption column, *Adsorpt. Sci. Technol.*, 19 (2001) 25–43.
- [53] Y. Lin, Z. Chen, Z. Chen, M. Megharaj, R. Naidu, Decoloration of acid violet red B by bentonite-supported nanoscale zero-valent iron: reactivity, characterization, kinetics and reaction pathway, *Appl. Clay Sci.*, 93–94 (2014) 56–61.
- [54] U.B. Simsek, M. Turabik, Decolorization mechanisms of an anionic dye by using zero-valent iron nanoparticles: application of response surface modeling for the optimization process, *Desal. Water Treat.*, 81 (2017) 303–314.
- [55] A. Ayar, O. Gezici, M. Küçükosmanoğlu, Adsorptive removal of Methylene blue and Methyl orange from aqueous media by carboxylated diaminoethane sporopollenin: on the usability of an aminocarboxylic acid functionality-bearing solid-stationary phase in column techniques, *J. Hazard. Mater.*, 146 (2007) 186–193.
- [56] J.L. Gong, Y.L. Zhang, Y. Jiang, G.M. Zeng, Z.H. Cui, K. Liu, C.H. Deng, Q.Y. Niu, J.H. Deng, S.Y. Huan, Continuous adsorption of Pb(II) and Methylene blue by engineered graphite oxide coated sand in fixed-bed column, *Appl. Surf. Sci.*, 330 (2015) 148–157.
- [57] F.E. Soetaredjo, A. Kurniawan, L.K. Ong, D.R. Widagdyo, S. Ismajji, Investigation of the continuous flow sorption of heavy metals in a biomass-packed column: revisiting the Thomas design model for correlation of binary component systems, *RSC Adv.*, 4 (2014) 52856–52870.
- [58] V. Parimelazhagan, G. Jeppu, N. Rampal, Continuous fixed-bed column studies on Congo red dye adsorption-desorption using free and immobilized *Nelumbo nucifera* leaf adsorbent, *Polymers*, 14 (2022) 54, doi: 10.3390/polym14010054.
- [59] M. Hanbali, H. Holail, H. Hammud, Remediation of lead by pretreated red algae: adsorption isotherm, kinetic, column modeling and simulation studies, *Green Chem. Lett. Rev.*, 7 (2014) 342–358.
- [60] M.R. Samarghandi, M. Hadi, G. McKay, Breakthrough curve analysis for fixed-bed adsorption of azo dyes using novel pine cone-derived active carbon, *Adsorpt. Sci. Technol.*, 32 (2014) 791–806.
- [61] H. Patel, Fixed-bed column adsorption study: a comprehensive review, *Appl. Water Sci.*, 9 (2019), doi:10.1007/s13201-019-0927-7.
- [62] J.L. White, Interpretation of infrared spectra of soil minerals, *Soil Sci.*, 112 (1971) 22–31.
- [63] U. Adie Gilbert, I. Unuabonah Emmanuel, A. Adeyemo Adebajo, G. Adeyemi Olalere, Biosorptive removal of Pb²⁺ and Cd²⁺ onto novel biosorbent: defatted Carica papaya seeds, *Biomass Bioenergy*, 35 (2011) 2517–2525.
- [64] Mu. Naushad, T. Ahamad, G. Sharma, A.H. Al-Muhtaseb, A.B. Albadarin, M.M. Alam, Z.A. AlOthman, S.M. Alshehri, A.A. Ghfar, Synthesis and characterization of a new starch/SnO₂ nanocomposite for efficient adsorption of toxic Hg²⁺ metal ion, *Chem. Eng. J.*, 300 (2016) 306–316.
- [65] S. Wang, Y. Zhou, B. Gao, X. Wang, X. Yin, K. Feng, J. Wang, The sorptive and reductive capacities of biochar supported nanoscaled zero-valent iron (nZVI) in relation to its crystallite size, *Chemosphere*, 186 (2017) 495–500.